The Seasonal Variation of Tropical Transient Planetary Waves Appearing in a GFDL General Circulation Model

Y. HAYASHI AND D. G. GOLDER

Geophysical Fluid Dynamics Laboratory/NOAA, Princeton University, Princeton, NJ 08540

(Manuscript received 28 February 1979, in final form 28 November 1979)

ABSTRACT

The seasonal variation of tropical transient planetary waves appearing in an 11-layer GFDL general circulation model is investigated. Space-time power spectra are estimated for every month by use of the maximum entropy method which can be applied to a short time record. The identification of equatorial wave modes is confirmed by space-time rotary spectral analysis which resolves traveling vortices into clockwise and anticlockwise components as well as eastward and westward moving components. It is found that the model's stratospheric Kelvin and mixed Rossby-gravity waves attain their primary and secondary maxima around July and January, respectively.

1. Introduction

This paper is an extension of a previous space-time spectral analysis (Hayashi, 1974) of tropical transient planetary waves appearing in an 11-layer GFDL general circulation model. The present study uses 12 months of the model's output which includes the 4-month period analyzed in the previous study. For a review of observational and theoretical studies of tropical transient planetary waves, the reader is referred to the introduction of the previous paper. Details of the model's structure and the seasonal variation of the gross statistics of simulated tropical disturbances are described in Manabe *et al.* (1974).

In Hayashi (1974), a spectral analysis was made of the model's tropical disturbances during the period July–October with respect to their characteristic wavenumber and frequency, three-dimensional structure, energetics and their role in the general circulation. In order to clarify the cause of these waves, Hayashi and Golder (1978) conducted a series of control experiments by eliminating, one by one, the topography, midlatitude disturbances and condensational heating from a 13-layer GFDL general circulation model to identify the role of these effects.

The above studies were limited to the Northern Hemisphere summer season. According to Manabe *et al.* (1974) the eddy kinetic energy in the tropics of the model exhibits a significant seasonal variation. It will be of interest to analyze the seasonal behavior of equatorial transient planetary waves, since this kind of study is difficult to do with observed data which are limited in space and time. It is, however, beyond the scope of the present analysis to identify the cause of the seasonal variation or the generation of these waves for each season.

In the present paper we shall focus our attention on the seasonal variation of mixed Rossby-gravity waves and Kelvin waves observed by Yanai and Maruyama (1966) and Wallace and Kousky (1968), respectively, since these two waves are of primary importance in the equatorial stratosphere, although other types of transient waves such as easterly waves and equatorial Rossby waves are important in the troposphere.

For this purpose the space-time power spectra are estimated every month by use of the maximum entropy method which can be applied to a short time record [see Hayashi (1977) for the computational procedure]. In order to confirm the identity of mixed Rossby-gravity and Kelvin waves, a space-time rotary spectral analysis recently developed by Hayashi (1979) is applied to the data.

In Section 2, the seasonal variation of the mean zonal wind is described. In Sections 3 and 4, the seasonal variation of mixed Rossby-gravity and Kelvin waves are analyzed, respectively. In Section 5, conclusions and remarks are made. An appendix describes formulas for computing space-time rotary power spectra.

2. The mean zonal wind

Since seasonal fluctuations of planetary waves may be influenced by changes in the basic state, the seasonal variation of the zonal wind is first described.

Fig. 2.1 shows the latitude-height distribution of the model's mean zonal wind during July (a) and

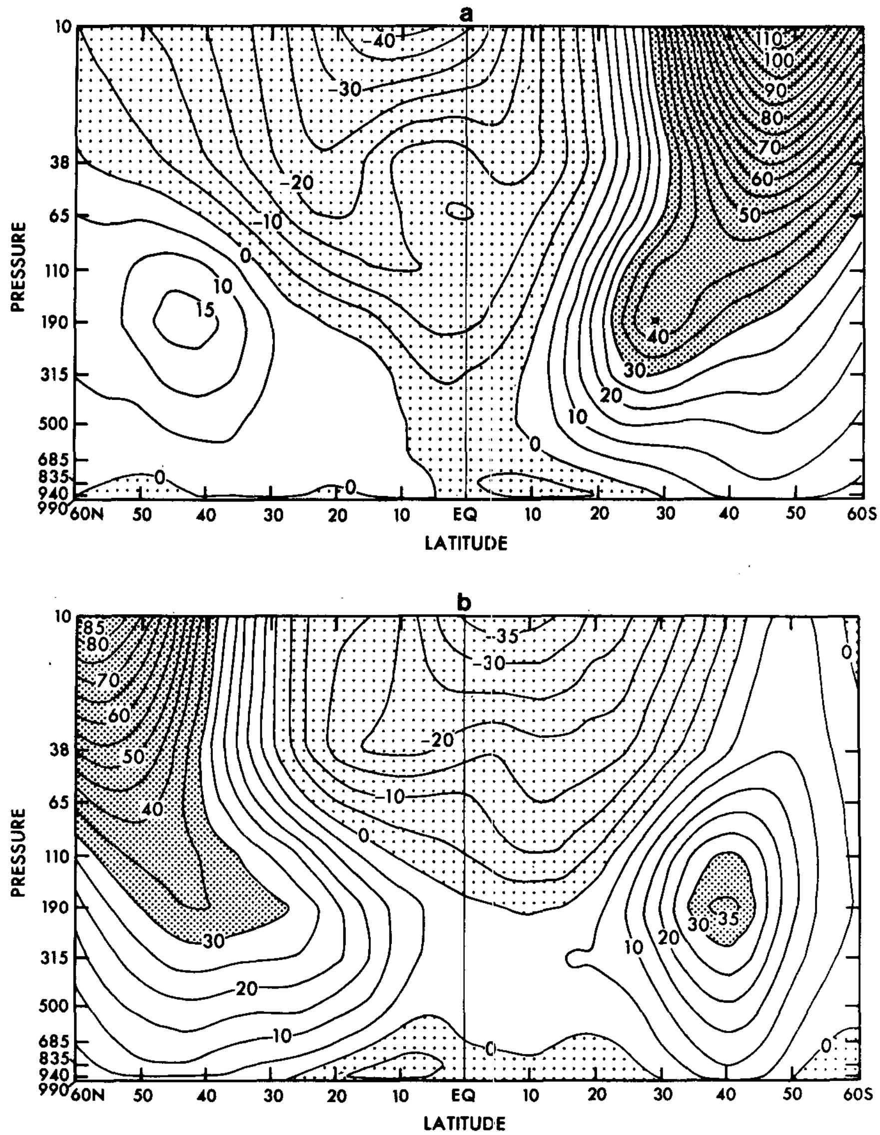

FIG. 2.1. Latitude-height distribution of the mean zonal wind in July (a) and January (b). Contour intervals 5 m s^{-1}.

January (b). Easterlies prevail over the equator although these easterlies are too weak in the lower troposphere and too strong in the stratosphere compared to those observed.[1] It should be noted here that the quasi-biennial oscillation of the stratospheric zonal wind is not simulated in this model, probably due to insufficient vertical resolution in the model's stratosphere. Strong westerlies are found in the winter hemisphere while weak westerlies are seen in the summer hemisphere.

The seasonal variation of the monthly mean zonal wind over the equator is shown in the time-height section of Fig. 2.2. The easterlies in the troposphere are strongest during the period July–August in agreement with observations. During October–May, weak westerlies appear in the upper troposphere in agreement with the observed zonal wind in the winters of 1958 and 1959 (Newell *et al.*, 1974, p. 208). However, the observed zonal wind consists of weak easterlies for the winters of 1960–65 (Newell *et al.*, 1969). According to Oort (1978), the tropical westerlies in this model are significantly reduced if grid points corresponding to available observational stations are sampled to compute the zonal mean.

Fig. 2.3 shows the monthly mean zonal wind in a time-latitude domain at the 110 mb level. The easter-

[1] See Manabe and Mahlman (1976, Fig. 4.1) for a distribution of the observed mean zonal wind averaged over seven years, based on Newell *et al.*, 1969.

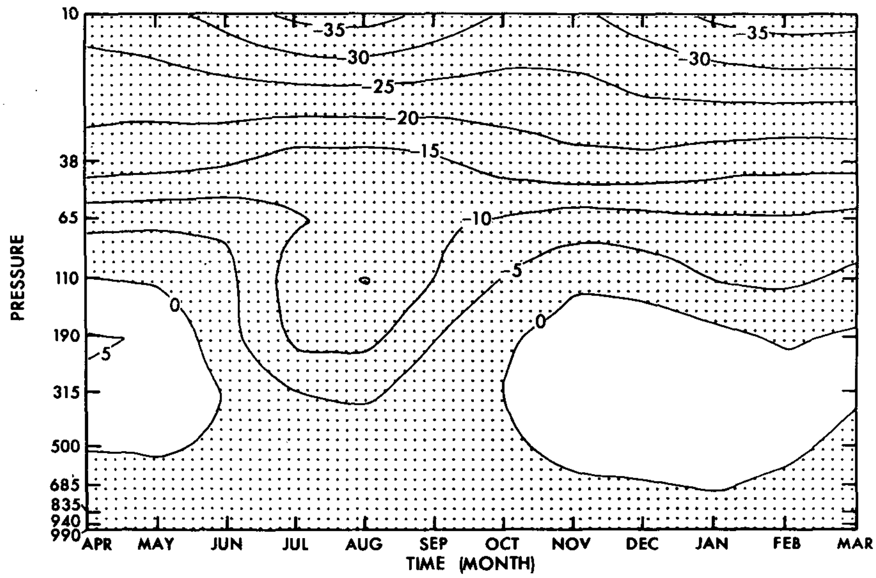

FIG. 2.2. Time-height section of the monthly mean zonal wind at the equator. Contour interval 5 m s^{-1}.

lies over the equator appear the strongest during July and August and are also strong during January and February. The westerlies attain their maxima in the midlatitudes during each hemispheric winter.

3. The mixed Rossby-gravity wave

a. Structure

Mixed Rossby-gravity waves observed by Yanai and Maruyama (1966) are characterized by a large meridional component at wavenumbers 3–5, periods of 4–6 days and move westward [M3–5, P4–6, W][2] as illustrated in the wavenumber-frequency diagram (Fig. 3.1) of the power spectrum of the model's meridional component at 110 mb over the equator during July.

Fig. 3.2 shows a latitude-height distribution of the power spectrum [M3–5, P4–6, W] of the meridional component during July. The maximum at the tropopause (110 mb) corresponds to mixed Rossby-

[2] Hereafter, M and P denote wavenumber and period (days) ranges, respectively, and E and W denote eastward and westward moving, respectively.

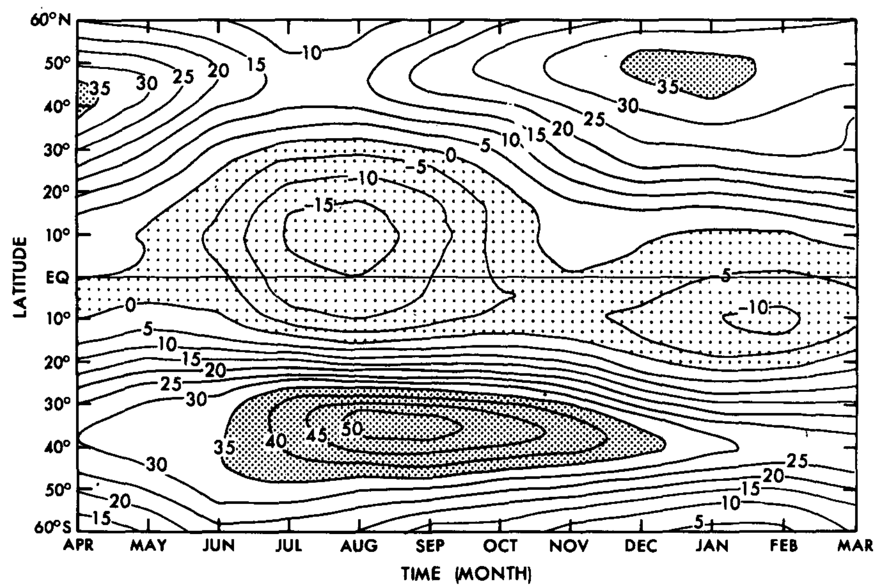

FIG. 2.3. Time-latitude section of the monthly mean zonal wind at 110 mb. Contour interval 5 m s^{-1}.

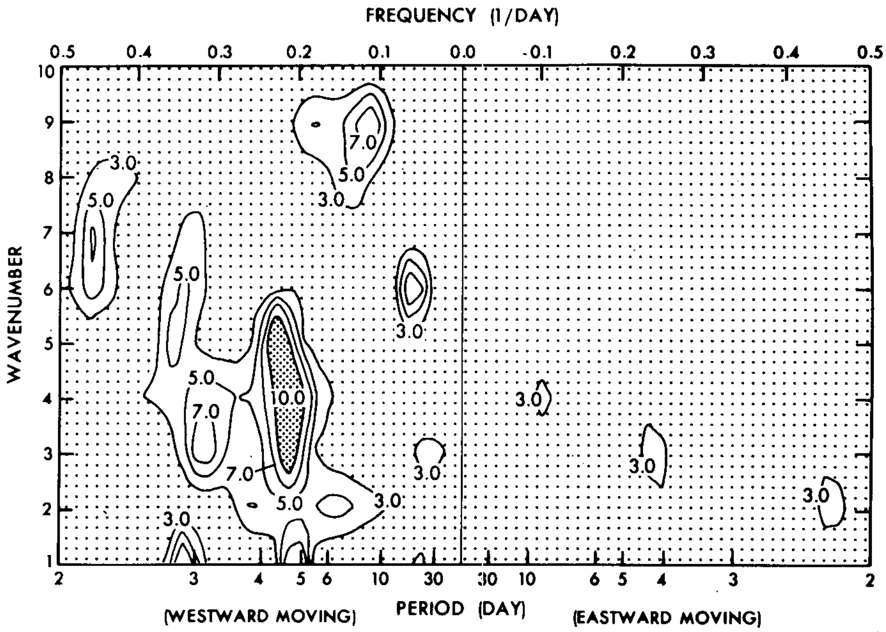

FIG. 3.1. Wavenumber-frequency diagram of power spectrum density ($m^2\ s^{-2}$ day) of the meridional component at 110 mb over the equator for July.

gravity waves. At 190 mb another maximum appears in the subtropics. However, this maximum is not clearly detected in other months. See Hayashi (1974) for a detailed description of the structure of these waves during the period July–October.

b. Seasonal variation

In order to document the seasonal variation of mixed Rossby-gravity waves, the power spectrum [M3–5] of the meridional component at 110 mb over the equator in the frequency-time domain is shown in Fig. 3.3. It is seen that westward moving mixed Rossby-gravity waves with periods of 4 to 6 days appear strongest during June–August. They can also be detected during November–December. These waves have the largest amplitude at the tropopause level throughout the year as illustrated by a time-height section (Fig. 3.4) of the power spectrum [M3–5, P4–6, W] of the meridional component.

Fig. 3.5a shows a time-latitude section of the power spectrum [M3–5, P3–6, W] of the meridional

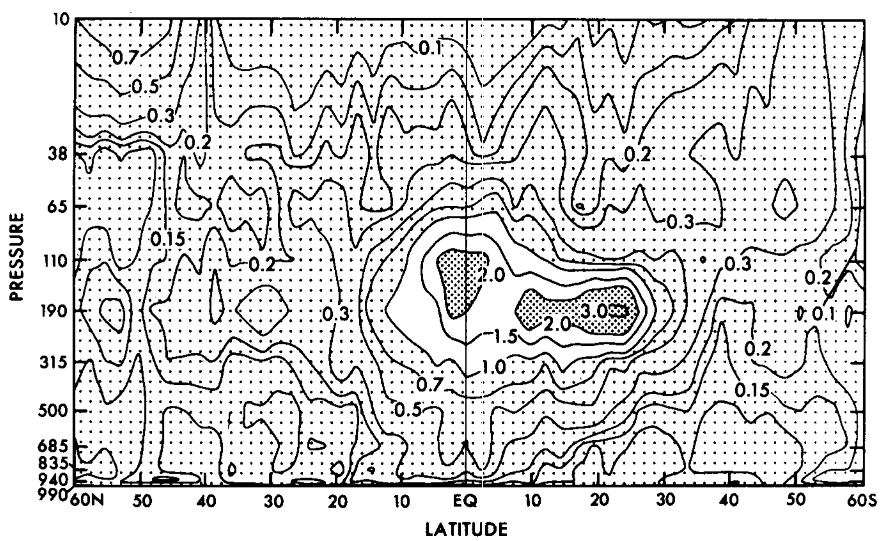

FIG. 3.2. Latitude-height distribution of power spectrum ($m^2\ s^{-2}$) for wavenumbers 3–5 and periods 4–6 days (westward moving) of the meridional component for July.

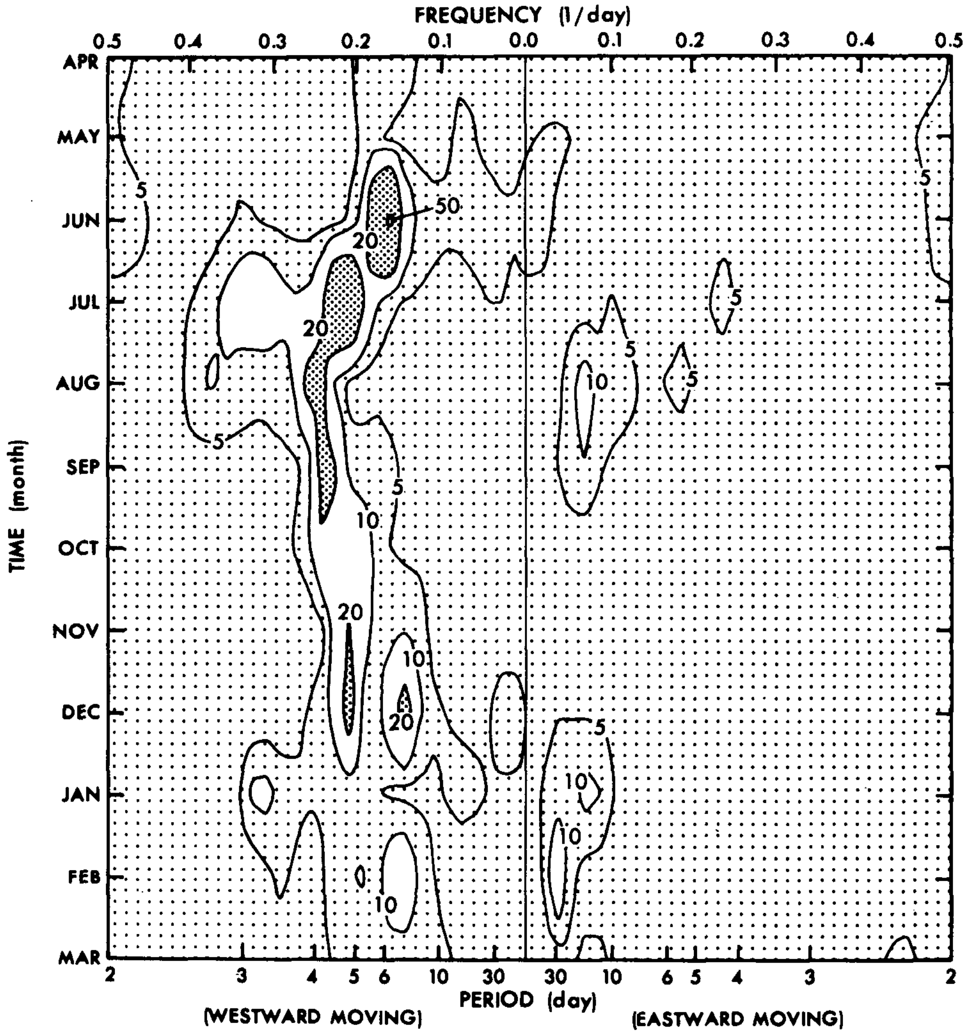

FIG. 3.3. Frequency-time section of power spectrum density ($m^2 s^{-2}$ day) for wavenumbers 3–5 of the meridional component at 110 mb over the equator.

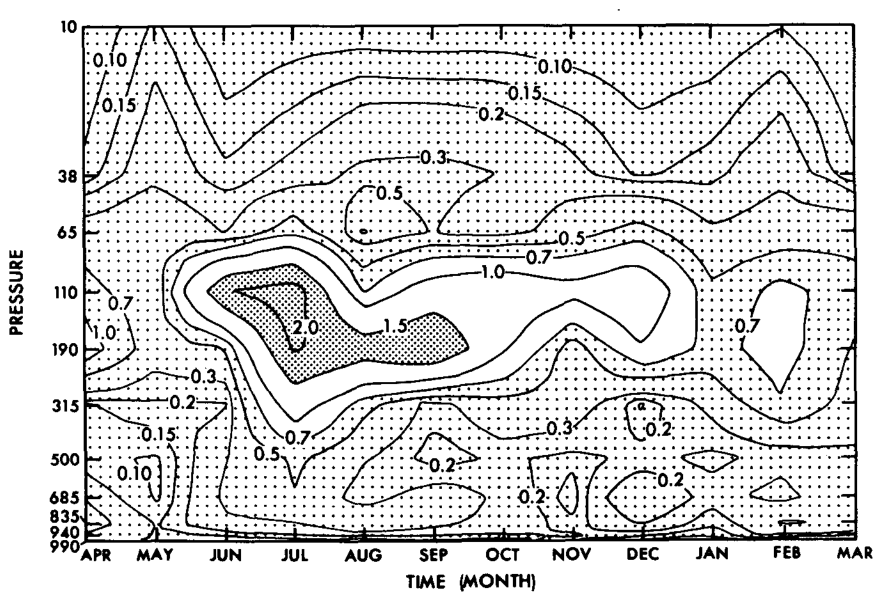

FIG. 3.4. Time-height section of power spectrum ($m^2 s^{-2}$) for wavenumbers 3–5, periods 4–6 days (westward moving) of the meridional component over the equator.

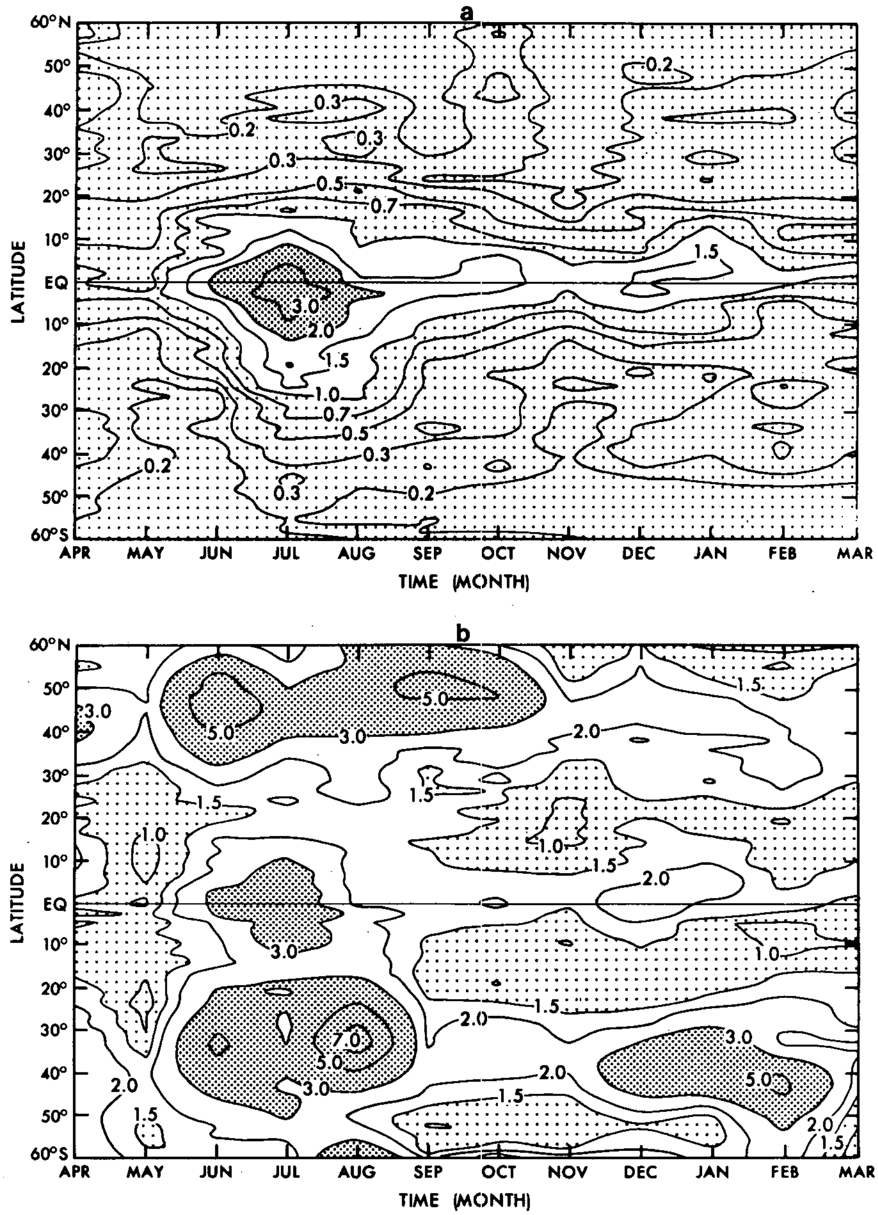

FIG. 3.5. Time-latitude section of power spectrum ($m^2 s^{-2}$) for (a) wavenumbers 3–5 and periods 3–6 days (westward moving) of the meridional component at 110 mb, and for (b), period range 3–20 days (westward moving).

component at 110 mb. The amplitude is confined to a narrow latitude belt centered on the equator throughout the year, and is consistent with the mixed Rossby-gravity wave pattern. Hayashi and Golder (1978) demonstrated that mixed Rossby-gravity waves during June and July are generated, to some extent, by condensation in the tropics, while they are significantly enhanced by equatorward propagation of midlatitude disturbances. Since midlatitude disturbances are associated with a wider frequency range than that of mixed Rossby-gravity waves found over the equator, Fig. 3.5b shows an analogous time-latitude section for [P3–20, W]. A large meridional component is seen, not only in the tropics, but also in the midlatitudes. The seasonal variation of mixed Rossby-gravity waves may be influenced by midlatitude disturbances, although no exact correspondence is found between the two. Their seasonal variation may also be related to that of the zonal wind (see Fig. 2.3) which affects the propagation of midlatitude disturbances. It should be mentioned that although the *westward* moving component (Fig. 3.5b) in midlatitudes is not stronger in winter than summer, the *eastward* moving component (not illustrated) is much stronger in winter than in sum-

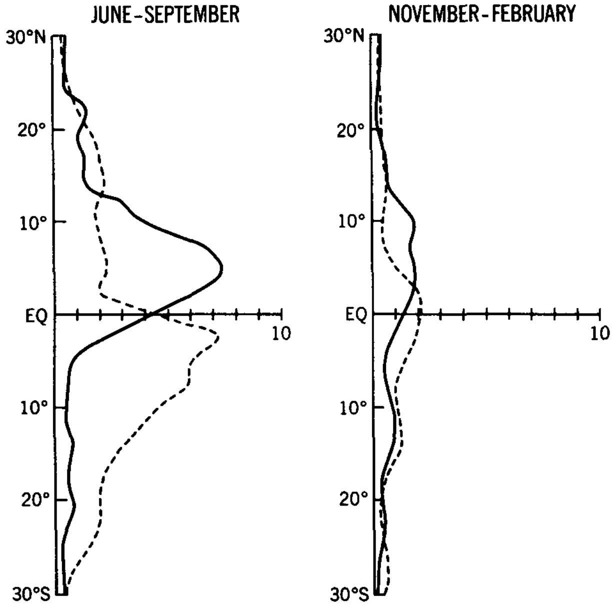

FIG. 3.6. Latitudinal distribution (110 mb level) of the space-time rotary power spectral density ($m^2 s^{-2}$ day) for June–September (left) and November–February (right) of the horizontal wind of wavenumber 4, period of 4 days (westward moving). Solid and dotted lines denote clockwise and anticlockwise components, respectively.

mer, in agreement with baroclinically unstable waves.

c. Space-time rotary spectral analysis

In order to confirm the identification of the above westward moving component with mixed Rossby waves, the wind vector is resolved into clockwise and anticlockwise rotating components, as well as eastward and westward propagating components by use of space-time rotary spectral analysis (see Appendix).

Since normal mode mixed Rossby-gravity waves (Matsuno, 1966) are characterized by westward moving vortices centered over the equator, their wind vectors should rotate with time, clockwise north of the equator and anticlockwise south of the equator.

Fig. 3.6 shows the latitudinal distribution of the space-time rotary power spectrum density [M4, P4, W] computed by the lag correlation method. During the period June through September (left), the clockwise component is dominant over the anticlockwise component in the Northern Hemisphere, while in the Southern Hemisphere the anticlockwise component dominates the clockwise component, as should be the case for mixed Rossby-gravity waves. During the period November–February (right), the same feature is found except that the amplitude is smaller and the clockwise and anticlockwise components have an equal amplitude a few degrees north of the equator. This implies that the center of the vortex is a little off the equator during this period, probably due to the asymmetry in the horizontal shear (see Fig. 2.1b) with respect to the equator.

4. The Kelvin wave

a. Structure

Kelvin waves observed by Wallace and Kousky (1968) are characterized by wavenumbers 1–2 with periods of 10–20 days and move eastward [M1–2,

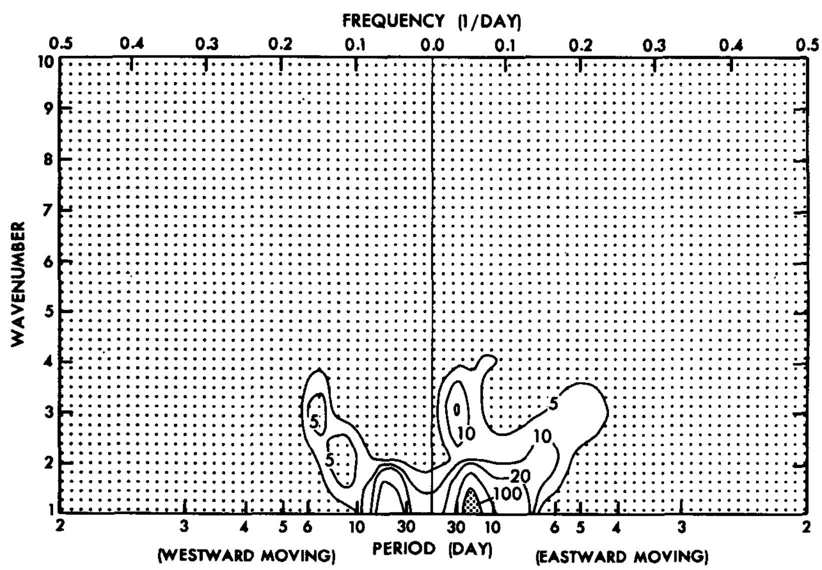

FIG. 4.1. Wavenumber-frequency diagram of the power spectrum density ($m^2 s^{-2}$ day) of the zonal component at 38 mb over the equator for July.

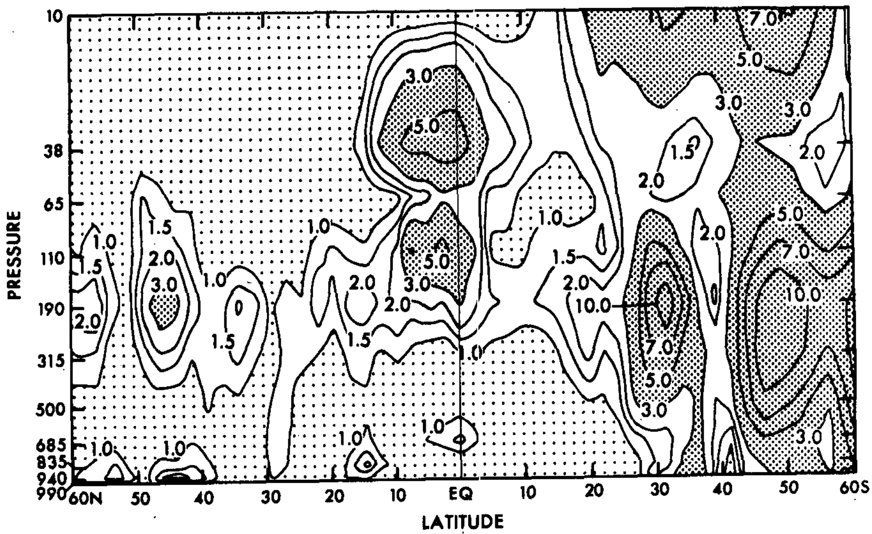

FIG. 4.2. Latitude-height distribution of power spectrum ($m^2\ s^{-2}$) integrated over wavenumbers 1–2 and periods 10–20 days (eastward moving) of zonal component for July.

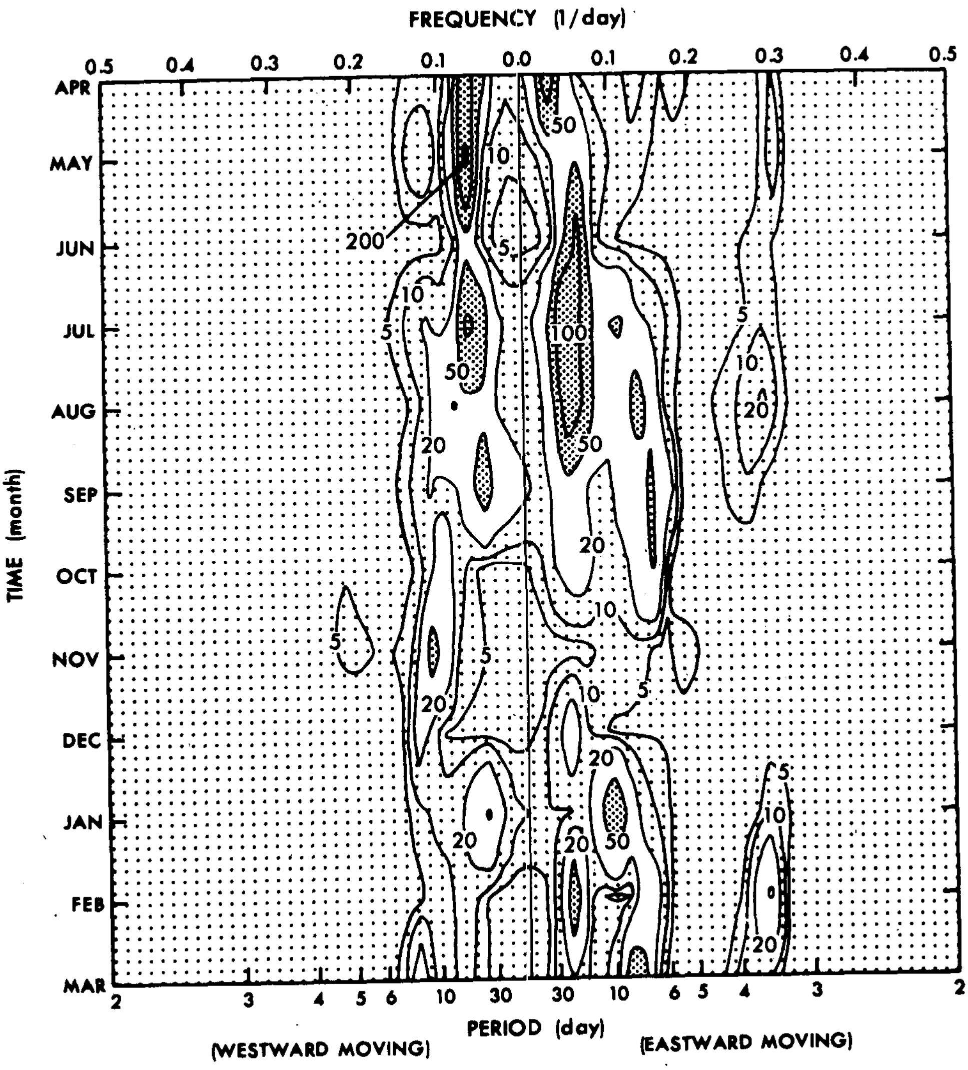

FIG. 4.3. Frequency-time section of power spectrum density ($m^2\ s^{-2}$ day) integrated over wavenumbers 1–2 of the zonal component at 38 mb over the equator.

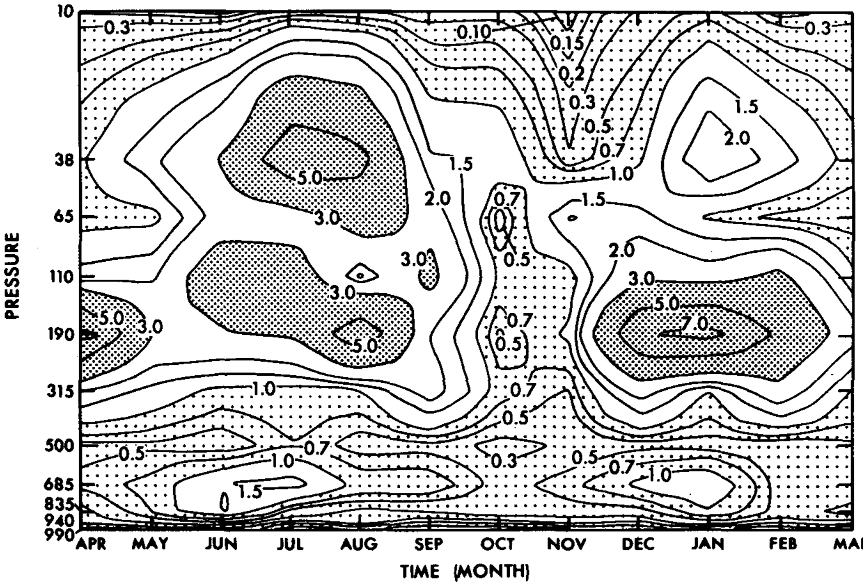

FIG. 4.4. Time-height section of power spectrum ($m^2 s^{-2}$) for wavenumbers 1–2, periods 10–20 days (eastward moving) of the zonal component over the equator.

P10–20, E] as illustrated in the wavenumber-frequency diagram (Fig. 4.1) of the space-time power spectrum of the model's zonal component at the 38 mb level over the equator during July.

Fig. 4.2 shows a latitude-height distribution of the power spectra in the wavenumber-frequency range [M1–2, P10–20, E] of the zonal component for July. The maxima at 38 and 110 mb confined to a narrow latitude belt centered on the equator correspond to Kelvin waves. This identification is supported by the fact that the power spectrum of the meridional wind is extremely small (not illustrated). For a detailed description of the structure of these waves during the period July–October, see Hayashi (1974).

b. Seasonal variation

The seasonal variation of the space-time power spectrum [M1–2] of the zonal component at 38 mb over the equator is shown in a frequency-time section (Fig. 4.3). It is seen that the eastward moving component with periods of 10–20 days appears strongest during the period June–August and can also be detected during December–February. At a lower level (190 mb), this component appears stronger during the latter period than it does in the former as is shown in a time-height section (Fig. 4.4) of the zonal component [M1–2, P10–20, E] over the equator. It seems that only a small portion of this component propagates into the stratosphere during December–February, probably due to the effect of vertical wind shear. However, a critical level absorption is not expected, since the relative phase velocity does not change sign with height even if the wave travels eastward in the westerlies.

Fig. 4.5 shows a time-latitude section of the power spectrum [M1–2, P10–20, E] of the zonal component at 38 mb (a) and 190 mb (b). The amplitude is large near the equator throughout the year, and is consistent with the Kelvin wave pattern.

c. Rotary spectral analysis

In order to confirm the identification of the above eastward moving component as due to Kelvin waves, a space-time rotary spectral analysis has been made. Since normal mode Kelvin waves (Matsuno, 1966) are characterized by a rectilinear oscillation of their wind vector in the zonal direction, their clockwise and anticlockwise components should have equal amplitudes.

Fig. 4.6 shows the latitudinal distribution of the space-time rotary power spectrum density [M1, P20, E]. In both periods, June–September (left) and November–February (right), the clockwise and anticlockwise components show comparable magnitudes near the equator. Thus, during both periods the above eastward moving component is identified with Kelvin waves, although the amplitude is weaker in the latter period.

5. Conclusions and remarks

Based on a space-time spectral analysis, the following conclusions have been reached concerning the seasonal variation of tropical transient planetary waves simulated by a GFDL general circulation model:

1) The model's easterlies in the equatorial troposphere are strongest during July–September,

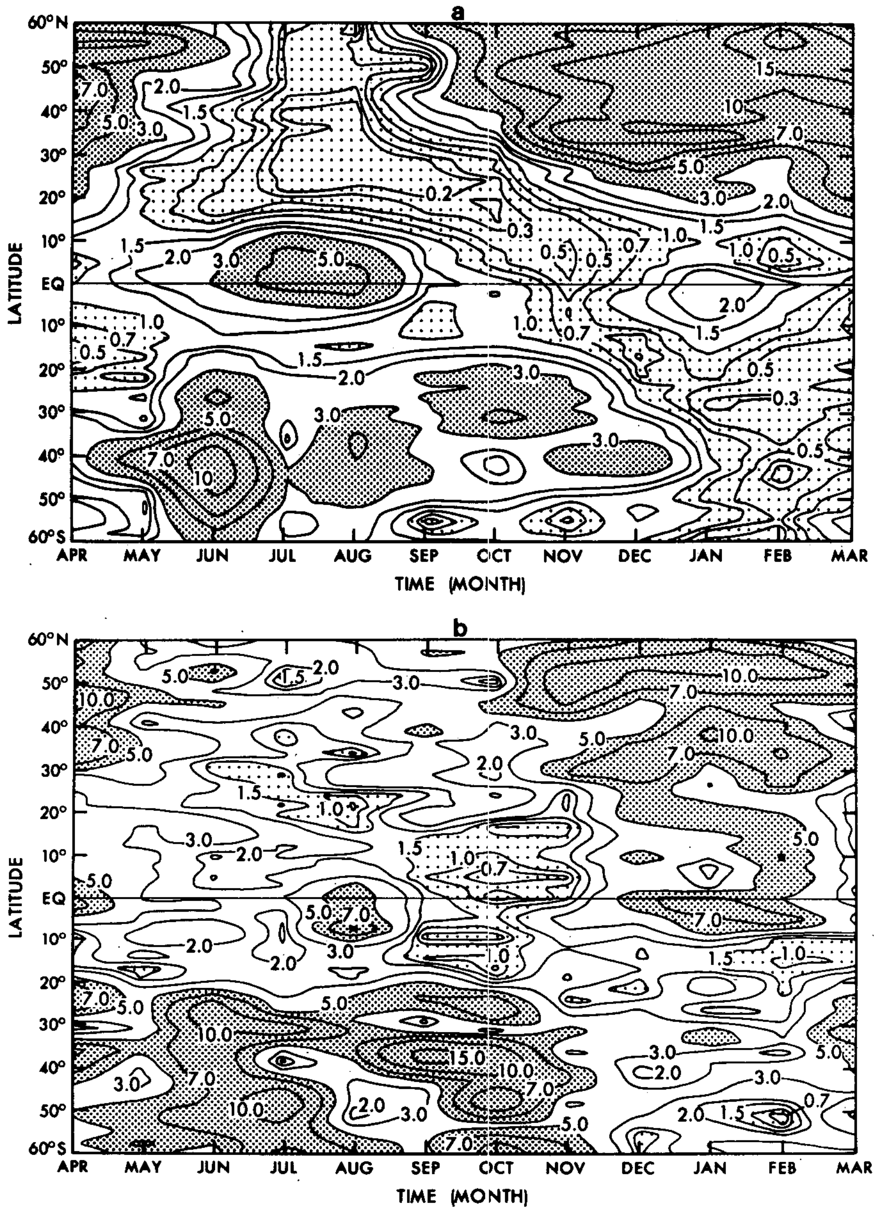

FIG. 4.5. Time-latitude section of power spectrum ($m^2\ s^{-2}$) for wavenumbers 1–2 and periods 10–20 days (eastward moving) of the zonal component at 38 mb (a) and 190 mb (b).

in agreement with those observed. In October–May weak westerlies appear in the equatorial upper troposphere, in agreement with those observed in 1958 and 1959.

2) The model's mixed Rossby-gravity waves are associated with wavenumbers 3–5 and periods 4–6 days and move westward throughout the year. They are characterized by clockwise and anticlockwise rotation of the wind vector in the Northern and Southern Hemispheres, respectively, being consistent with their theoretical normal mode wave pattern. They attain their primary and secondary maximum amplitudes around July and January, respectively, at the tropopause level.

3) The model's Kelvin waves are associated with wavenumbers 1–2 and periods 10–20 days and move eastward throughout the year. They are characterized by an equal magnitude of clockwise and anticlockwise rotating wind components, being consistent with their theoretical normal mode pattern. They attain their primary and secondary maximum amplitudes around July and January, respectively, in the stratosphere (38 mb), whereas their amplitude is large during both July and January in the troposphere.

The fact that the model's equatorial waves attain two maxima during one year may well be related to

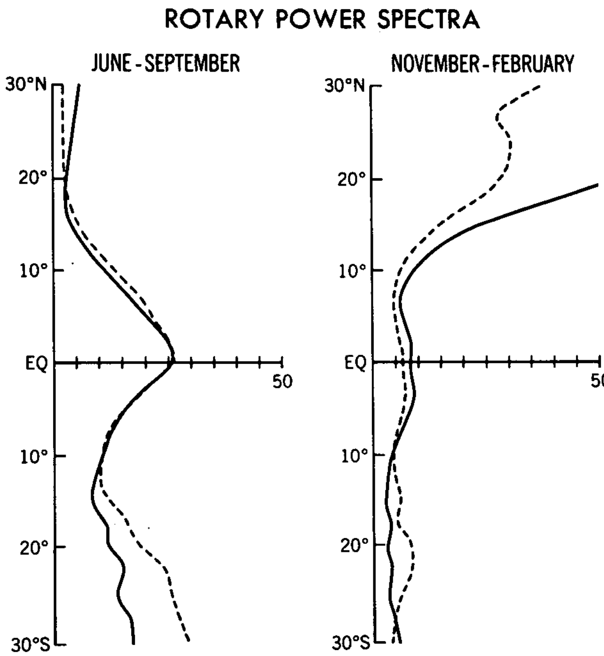

FIG. 4.6. Latitudinal distribution (38 mb level) of the space-time rotary power spectral density ($m^2 s^{-2}$ day) for June–September (left) and November–February (right) of the horizontal wind of wavenumber 1, period of 20 days (eastward moving). Solid and dotted lines show clockwise and anticlockwise components, respectively.

the sun crossing over the equator twice a year. On the other hand, the finding that these two maxima are not of the same magnitude must be ultimately related to the asymmetry between the geography of both hemispheres through the seasonal variation in the zonal mean state, precipitation, and the amplitude of midlatitude disturbances. According to Manabe *et al.* (1974) the seasonal variation of precipitation in the present model is closely related to the sea surface temperature which is prescribed seasonally, based on that observed. The effect of sea surface temperature and precipitation on the seasonal variation of tropical disturbances can be identified by comparing models with and without a seasonal variation in the sea surface temperature. However, this comparison is beyond the scope of the present study.

Our analysis suggests the presence of both semiannual and annual cycles in Kelvin and mixed Rossby-gravity waves, although Maruyama (1971) could not clearly detect these cycles in stratospheric and tropospheric disturbances by use of observed time-series data. These cycles may be detected observationally by using the space-time series data which will be available from the 1979 Global Weather Experiment. Hirota (1978, 1979) clearly detected a semiannual cycle in observed mesospheric Kelvin waves. In the real atmosphere, stratospheric Kelvin and mixed Rossby-gravity waves do not appear with great strength in the same year (see Maruyama, 1969, 1979), probably due to the quasi-biennial oscillation of the stratospheric zonal wind which is not simulated in the present model. In order to simulate the interannual variability of the tropical stratospheric circulation, a model with finer vertical resolution is warranted.

Acknowledgments. The authors wish to express their hearty appreciation to Dr. S. Manabe for his valuable suggestions and comments. We are grateful to Drs. K. Miyakoda, J. D. Mahlman for their critical review and to Dr. J. Smagorinsky for his interest and encouragement. We are also indebted to the anonymous reviewers for their valuable comments on the original version of this paper. Thanks are extended to P. Tunison for drafting, J. Conner for photography and E. Thompson and J. Kennedy for typing.

APPENDIX

Space-Time Rotary Power Spectra

The rotary vector $\mathbf{w}$ is defined as a complex vector given by

$$\mathbf{w}(x,t) = \mathbf{u}(x,t) + i\mathbf{v}(x,t), \qquad \text{(A1)}$$

where $\mathbf{u}$ and $\mathbf{v}$ are the zonal and meridional velocities, while x and t are longitude and time, respectively.

The space-time rotary power spectrum $P_{k,f}(\mathbf{w})$ is defined as a space-time power spectrum of the rotary vector and is computed through the formulas (Hayashi, 1979)

$$2P_{\pm k,\pm f}(\mathbf{w}) = P_{\pm f}(W_{\pm k}), \qquad \text{(A2a)}$$

$$= P_{\pm k,\pm f}(\mathbf{u}) + P_{\pm k,\pm f}(\mathbf{v}) - 2Q_{\pm k,\pm f}(\mathbf{u},\mathbf{v}), \qquad \text{(A2b)}$$

where P_f in (A2a) is the time power spectrum of a complex variable and W_k is the complex space-Fourier transform of $\mathbf{w}$, while $P_{k,f}$ and $Q_{k,f}$ in (A2b) are the space-time power and quadrature spectra, respectively.

The positive value of the frequency f corresponds to anticlockwise rotation of the rotary vector with time, a negative value denoting a clockwise rotation. One period corresponds to one rotation of the vector in a complex plane. The positive value of f/k corresponds to westward phase velocity, while a negative value corresponds to an eastward phase velocity.

Eq. (A2a) given in complex representation is suitable for applying the maximum entropy method to compute the time power spectrum (see Hayashi, 1977), while (A2b) is convenient for applying conventional methods of computing space-time cross spectra (Hayashi, 1971).

REFERENCES

Hayashi, Y., 1971: A generalized method of resolving disturbances into progressive and retrogressive waves by space Fourier and time cross-spectral analyses. *J. Meteor. Soc. Japan*, **49**, 125–128.

——, 1974: Spectral analysis of tropical disturbances appearing in a GFDL general circulation model. *J. Atmos. Sci.*, **31**, 180–218.

——, 1977: Space-time spectral analysis using the maximum entropy method. *J. Meteor. Soc. Japan*, **55**, 415–420.

——, 1979: Space-time spectral analysis of rotary vector series. *J. Atmos. Sci.*, **36**, 757–766.

——, and D. G. Golder, 1977: Space-time spectral analysis of midlatitude disturbances appearing in a GFDL general circulation model. *J. Atmos. Sci.*, **34**, 237–262.

——, and ——, 1978: The generation of equatorial transient planetary waves: Control experiments with a GFDL general circulation model. *J. Atmos. Sci.*, **35**, 2068–2082.

Hirota, I., 1978: Equatorial waves in the upper stratosphere and mesosphere in relation to the semiannual oscillation of the zonal wind. *J. Atmos. Sci.*, **35**, 714–722.

——, 1979: Kelvin waves in the equatorial middle atmosphere observed by the Nimbus 5 SCR. *J. Atmos. Sci.*, **36**, 217–222.

Manabe, S., and J. D. Mahlman, 1976: Simulation of seasonal and interhemispheric variations in the stratospheric circulation. *J. Atmos. Sci.*, **33**, 2185–2217.

——, D. G. Hahn and J. L. Holloway, Jr., 1974: The seasonal variation of the tropical circulation as simulated by a global model of the atmosphere. *J. Atmos. Sci.*, **31**, 43–83.

Maruyama, T., 1969: Long-term behavior of Kelvin waves and mixed Rossby-gravity waves. *J. Meteor. Soc. Japan*, **47**, 245–254.

——, 1971: Vertical section and time sequence of spectra of disturbances over the Line Islands during the years 1957–1958. *J. Meteor. Soc. Japan*, **49**, 146–157.

——, 1979: Equatorial wave intensity over the Indian Ocean during the years 1968–1972. *J. Meteor. Soc. Japan*, **57**, 39–51.

Matsuno, T. 1966: Quasi-geostrophic motions in the equatorial area. *J. Meteor. Soc. Japan*, **44**, 25–43.

Newell, R. E., D. G. Vincent, T. G. Dopplick, D. Ferruzza and J. W. Kidson, 1969: The energy balance of the global atmosphere. *The Global Circulation of the Atmosphere*, G. A. Corby, Ed., Roy. Meteor. Soc., 42–90.

——, J. W. Kidson, D. G. Vincent and G. J. Boer, 1974: *The General Circulation of the Tropical Atmosphere*, Vol. 2. The MIT Press, 371 pp.

Oort, A. H., 1978: Adequacy of rawinsonde network for global circulation studies tested through numerical output. *Mon. Wea. Rev.*, **106**, 174–195.

Wallace, J. M., and V. E. Kousky, 1968: Observational evidence of Kelvin waves in the tropical stratosphere. *J. Atmos. Sci.*, **95**, 900–907.

Yanai, M., and T. Maruyama, 1966: Stratospheric wave disturbances propagating over the equatorial Pacific. *J. Meteor. Soc. Japan*, **44**, 291–294.